Research Square

Preprints are preliminary reports that have not undergone peer review.
They should not be considered conclusive, used to inform clinical practice,
or referenced by the media as validated information.

Nonlinear dynamic analysis of an optoelectronic-oscillator-based joint radar-communication system

Alex B. N. Pefireko
Universidade Federal Fluminense
Vitor T. Ferreira
Universidade Federal Fluminense
José R. M. Andrade
Universidade Federal Fluminense
M. C.R. Frauche
Universidade Federal Fluminense
Fabiolat-Winifred T. Fouotsop
Unité de Recherche d'Automatique et Informatique Appliquée (UR-AIA), Fotso Victor University Institute of Technology, University of Dschang
Vanessa P. M. Ribeiro
Universidade Federal Fluminense
Isidore Z. Djoufack
Unité de Recherche d'Automatique et Informatique Appliquée (UR-AIA), Fotso Victor University Institute of Technology, University of Dschang
Cláudia B. Marcondes
CEFET/RJ
Alexandre C. T. Santos
Universidade Federal Fluminense
Jimmi H. Talla Mbé
University of Dschang
Ricardo M. Ribeiro
rmribeiro@id.uff.br
Universidade Federal Fluminense

Research Article

Keywords: Optoelectronic oscillator, Joint radar–communication, Nonlinear dynamics, Chaos, Microwave photonics, Intelligent transportation systems, Largest Lyapunov exponent

Posted Date: November 16th, 2026

DOI: https://doi.org/10.21203/rs.3.rs-11473676/v1

License: This work is licensed under a Creative Commons Attribution 4.0 International License.
Read Full License

Additional Declarations: No competing interests reported.

Nonlinear dynamic analysis of an optoelectronic-oscillator-based joint radar-communication system

Alex B. N. Pefireko[1,2], Vitor T. Ferreira[1], José R. M. Andrade[1], M. C. R. Frauche[1], Fabiolat-W. Foutsop Tiaya[4,5], Vanessa P. M. Ribeiro[1], Zacharie I. Djoufack[4], Cláudia B. Marcondes[2], Alexandre C. T. Santos[1], Jimmi H. Talla Mbé[3], Ricardo M. Ribeiro[1*]

[1*]Laboratório de Comunicações Ópticas, Laboratório de Antenas e Propagação, Departamento de Engenharia de Telecomunicações, Universidade Federal Fluminense, 24210-240, Niterói, RJ, Brazil.
[2]Laboratório de Física Experimental e Aplicada, Departamento de Física, CEFET/RJ, 20271-110, Rio de Janeiro, RJ, Brazil.
[3]Research Unit of Condensed Matter, Electronics and Signal Processing, Department of Physics, University of Dschang, 67, Dschang, Cameroon.
[4]Unité de Recherche d'Automatique et Informatique Appliquée (UR-AIA), Fotso Victor University Institute of Technology, University of Dschang, 134, Bandjoun, Cameroon.
[5]Research Institute on Mines and the Environment (RIME), University of Quebec in Abitibi-Témiscamingue (UQAT), J9X 5E4, Rouyn-Noranda, QC, Canada.

*Corresponding author(s). E-mail(s): rmribeiro@id.uff.br;
Contributing authors: alex.pefireko@aluno.cefet-rj.br; vitor_tavares@id.uff.br; moraesjose@id.uff.br; mfrauche@id.uff.br; tiayafabiolat010@gmail.com; vanessamagri@id.uff.br; djoufackzacharie@yahoo.fr; claudia.marcondes@cefet-rj.br; alexandre.toledo@aluno.cefet-rj.br; jimmi.talla-mbe@univ-dschang.org;

Abstract

This paper presents a comprehensive analytical and numerical investigation of the nonlinear dynamics of an optoelectronic oscillator (OEO)-based joint radar–communication (JRC) architecture under binary and sinusoidal IQ modulation. Although OEO-based JRC systems have recently attracted considerable attention, the influence of communication waveforms on the nonlinear dynamics of the delayed feedback loop remains insufficiently explored. To address this issue, a delay-differential model is established and combined with linear stability analysis to determine the critical oscillation frequency and feedback gain. The results reveal that the communication waveform actively influences the dynamical behavior of the OEO in addition to the feedback gain. Under binary IQ modulation, variations in the I- and Q-channel bit rates produce only a limited modification of the dynamical regime, while chaotic operation remains robust over the investigated transmission-rate range at sufficiently high feedback gain. In contrast, sinusoidal IQ modulation introduces the I- and Q-channel frequencies as additional dynamical control parameters, leading to frequency-dependent stable and chaotic regions. Furthermore, assigning distinct carrier frequencies to the two channels extends the stable operating region and produces a richer spectral response, while the information-bearing frequency components remain identifiable after the onset of chaotic dynamics. These results provide new physical insight into the interaction between communication waveforms and delayed nonlinear photonic oscillators. More importantly, they show that IQ modulation can influence not only the transmitted information but also the dynamical state of the OEO. The resulting stability maps provide a practical framework for relating the feedback gain and communication parameters to the desired dynamical regime, thereby establishing useful design guidelines for OEO-based JRC systems.

Keywords: Optoelectronic oscillator, Joint radar–communication, Nonlinear dynamics, Chaos, Microwave photonics, Intelligent transportation systems, Largest Lyapunov exponent

1 Introduction

The rapid increase in vehicle density has intensified the demand for intelligent transportation infrastructures capable of ensuring road safety, reducing traffic congestion, and improving energy efficiency [1]. Intelligent transportation systems (ITS) have consequently emerged as an effective solution by integrating sensing, communication, and control technologies to enhance traffic efficiency, safety, and environmental sustainability [2].

A key requirement of ITS is the ability to simultaneously sense the surrounding environment while exchanging information with nearby vehicles and infrastructure. Traditionally, these tasks are performed by independent radar and communication subsystems. While radar provides accurate target detection, ranging, and velocity estimation [3], its sensing capabilities are also relevant to a broader range of applications, including road-user and obstacle monitoring as well as the detection and tracking of airborne targets such as airplanes and drones. Wireless

communications, meanwhile, enable vehicle-to-vehicle (V2V), vehicle-to-infrastructure (V2I), and vehicle-to-everything (V2X) connectivity [4]. However, implementing these functions separately increases hardware complexity, power consumption, cost, and spectrum occupancy [5–7]. These limitations have stimulated the development of joint radar–communication (JRC) systems, which integrate sensing and communication functionalities within a common hardware platform while sharing spectral resources [8–10].

Among the various photonic technologies proposed for JRC applications, optoelectronic oscillators (OEOs) have attracted considerable attention owing to their capability to generate ultra-low-phase-noise microwave signals with excellent spectral purity and outstanding frequency stability [11, 12]. The delayed optoelectronic feedback loop inherent to OEOs provides an exceptionally high quality factor that is difficult to achieve using purely electronic oscillators, making them particularly attractive for microwave photonics, high-performance communication systems, and photonic radar applications [13, 14]. More recently, chaotic OEO architectures have also been explored for multifunctional radar–communication systems, further highlighting their potential for integrated photonic sensing and communication [15, 16].

Besides their microwave generation capability, OEOs have also emerged as versatile photonic platforms for sensing and measurement applications. Their exceptional frequency stability enables physical quantities to be converted into measurable microwave frequency shifts, leading to high-resolution optical sensing techniques for parameters such as temperature, refractive index, and liquid level [17]. In this context, OEO-based sensing architectures have been theoretically investigated for the simultaneous measurement of several liquid physical parameters, demonstrating that the nonlinear oscillator characteristics can significantly enhance measurement sensitivity [18, 19]. These developments further emphasize that the dynamical behavior of an OEO is intrinsically linked to its practical performance. From a nonlinear dynamics perspective, delayed OEOs are known to exhibit a wide variety of operating regimes, including periodic oscillations, bifurcations, quasi-periodicity, and chaos depending on the system parameters [20–23]. Such nonlinear regimes directly affect oscillation stability, spectral purity, and waveform predictability, making their understanding essential for both sensing and joint radar–communication applications.

In parallel, OEOs have also been extensively investigated for microwave photonic communication systems. Sinquin *et al.* demonstrated a directly modulated low-phase-noise OEO suitable for microwave communications [24], while Zeng *et al.* proposed an OEO capable of generating multiple microwave signal formats [25]. Building upon these developments, Xue *et al.* experimentally demonstrated a photonics-assisted JRC architecture integrating radar sensing and wireless communication within a single OEO platform [26]. Nevertheless, the OEO was assumed to operate in its nominal microwave generation regime, and the influence of the delayed nonlinear dynamics on the stability and operating conditions of the overall JRC system was not investigated.

Motivated by this research gap, this paper presents a comprehensive analytical and numerical investigation of the nonlinear dynamics of an OEO-based JRC architecture inspired by the configuration reported by Xue *et al.* [26]. A delay-differential model is first established and combined with linear stability analysis to derive the

critical oscillation frequency and feedback gain. The resulting analytical predictions are subsequently validated through bifurcation diagrams, largest Lyapunov exponent, time-domain responses, and power spectral density under different IQ modulation schemes.

To further clarify the interaction between communication waveforms and nonlinear dynamics, three-dimensional dynamic stability maps based on the largest Lyapunov exponent are constructed in both the communication bit-rate and modulation-frequency parameter spaces. These maps provide a global representation of the operating regimes and reveal that the communication parameters influence the oscillator dynamics in fundamentally different ways depending on the modulation format. While binary IQ modulation preserves the dynamical regime over a broad range of transmission bit rates, sinusoidal IQ modulation introduces frequency-dependent stability boundaries that can be exploited to tailor the nonlinear behavior of the OEO. More importantly, the results demonstrate that communication waveforms are not merely carriers of information but actively participate in shaping the dynamical operating regime of the oscillator. These findings provide new physical insight into OEO-based JRC systems and establish practical design guidelines for selecting the operating conditions according to the desired radar and communication functionalities.

The remainder of this paper is organized as follows. Section II presents the system architecture and the mathematical model. Section III develops the linear stability analysis. Section IV reports and discusses the nonlinear dynamics under different IQ modulation schemes. Finally, Section V concludes the paper.

2 System description and mathematical modeling

2.1 System architecture

The proposed joint radar–communication system is built upon an optoelectronic oscillator (OEO) architecture, as illustrated in Fig. 1 [26]. A continuous-wave (CW) optical carrier generated by a laser diode (LD) is first adjusted by a polarization controller (PC1), which aligns the input state of polarization with the operating axes of the dual-polarization dual-parallel Mach–Zehnder modulator (DPol-DPMZM). The DPol-DPMZM consists of two dual-parallel MZMs arranged along orthogonal polarization branches. The X-polarization branch is driven by the electrical feedback signal to sustain microwave oscillation, whereas the Y-polarization branch is excited by the in-phase (I) and quadrature (Q) modulation signals carrying the joint radar and communication information. The modulated optical signals are then recombined and pass through a second polarization controller (PC2), which optimizes the polarization state of the generated optical waveform before optical distribution. An optical coupler (OC) subsequently splits the optical power into two paths. One branch is directed toward the transmitter block for wireless radiation, while the other enters the OEO feedback loop. In this loop, the optical signal propagates through a single-mode fiber (SMF), introducing the delay T_D, which governs the oscillation frequency and contributes to the high quality factor of the oscillator. After photodetection (PD), the recovered

electrical signal is amplified by an electrical amplifier (EA) and filtered by an electrical bandpass filter (EBPF) to select the desired oscillation modes. An electrical coupler (EC) then extracts a fraction of the oscillating microwave signal for the receiver block, where radar echoes and communication signals are coherently processed. Simultaneously, the remaining electrical signal is applied to a 90° hybrid coupler, which generates the quadrature driving signals required by the X-DPMZM before being reinjected into the DPol-DPMZM, thereby closing the optoelectronic feedback loop and maintaining self-sustained microwave oscillation. Through this architecture, the same optoelectronic oscillator simultaneously provides the microwave waveform used for radar sensing and the carrier supporting wireless communication, enabling a compact and spectrally efficient photonic joint radar–communication system.

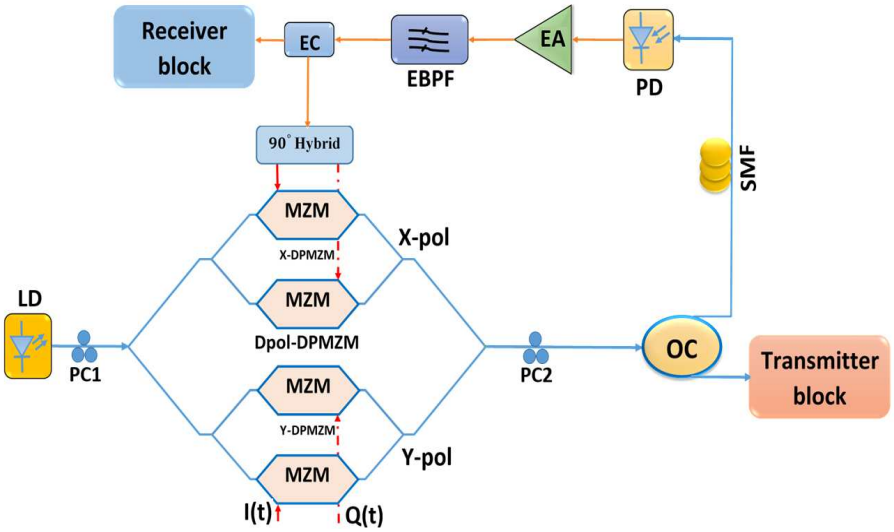


Figure 1: Architecture of the joint radar–communication system [26]. LD: laser diode; PC: polarization controller; Dpol-DPMZM: dual-polarization dual-parallel Mach–Zehnder modulator; DPMZM: dual-parallel Mach–Zehnder modulator; MZM: Mach–Zehnder modulator; X-pol and Y-pol: orthogonal polarization branches; OC: optical coupler; SMF: single-mode fiber; PD: photodiode; EA: electrical amplifier; EBPF: electrical bandpass filter; EC: electrical coupler; $I(t)$ and $Q(t)$: in-phase and quadrature modulation signals, respectively.

2.2 Mathematical model

The mathematical model of the JRC system is derived from the optoelectronic oscillator (OEO) incorporating a dual–polarization dual–parallel Mach–Zehnder modulator (Dpol–DPMZM). Let $V(t)$ denote the electrical feedback signal driving the X–polarized branch, and $I(t)$, $Q(t)$ the in-phase and quadrature modulation signals

applied to the Y–polarized branch. The DPMZM transfer function depends on the modulation index m:

$$m = \frac{\pi}{2.V_\pi}, \tag{1}$$

where V_π is the modulator half-wave voltage. The X-polarized branch is driven by the delayed feedback signal and is given as follows :

$$\begin{aligned} E_X(t) = \frac{\sqrt{2}}{2} E_{\text{in}}(t) \Big[& - j \sin(mV(t-\tau) + \phi) \\ & + \sin(mV(t-\tau) + \phi) \Big], \end{aligned} \tag{2}$$

where ϕ is the bias point and τ is the modulator electrical delay [27]. The Y-polarized branch, which is modulated by the in-phase and quadrature signals $I(t)$ and $Q(t)$, yields:

$$E_Y = \frac{\sqrt{2}}{2} E_{\text{in}}(t) \left[\sin\left(mI(t) + \phi\right) + j \sin\left(mQ(t) + \phi\right) \right]. \tag{3}$$

When the polarization controller (PC2) at the output of the DPol-DPMZM is set to 45°, the optical fields from the X- and Y-polarization branches combine to form the total optical output [27]:

$$\begin{aligned} E_{\text{out}} = \frac{\sqrt{2}}{2} E_{\text{in}}(t) \big[& - j \sin\left(mV(t-\tau) + \phi\right) + \\ & \sin\left(mV(t-\tau) + \phi\right) + \sin\left(mI(t) + \phi\right) + j \sin\left(mQ(t) + \phi\right) \big]. \end{aligned} \tag{4}$$

The detected optical power is :

$$\begin{aligned} P_{\text{out}} = \frac{1}{4} P_{\text{in}} \Big\{ & \sin^2\big(mV(t-\tau) + \phi\big) + \sin^2\big(mI(t) + \phi\big) \\ & + 2 \sin\big(mV(t-\tau) + \phi\big) \cdot \sin\big(mI(t) + \phi\big) + \sin^2\big(mQ(t) + \phi\big) \\ & + \sin^2\big(mV(t) + \phi\big) - 2 \sin\big(mQ(t) + \phi\big) \cdot \sin\big(mV(t) + \phi\big) \Big\}. \end{aligned} \tag{5}$$

Assuming small modulation indices for the IQ signals ($mI(t) \ll 1$ and $mQ(t) \ll 1$), together with modulation frequencies much lower than the oscillation frequency of the OEO ($f_I, f_Q \ll f_{\text{OEO}}$), the low-frequency components can be neglected after filtering, leading to the following simplified expression for the detected optical power:

$$\begin{aligned} P_{\text{out}} = \frac{1}{4} P_{\text{in}} \Big\{ & \sin^2\big(mV(t-\tau) + \phi\big) + \sin^2\big(mV(t) + \phi\big) \\ & + 2mI(t) \sin\big(mV(t-\tau) + \phi\big) - 2mQ(t) \sin\big(mV(t) + \phi\big) \Big\}. \end{aligned} \tag{6}$$

Following propagation through the optical fiber, the optical signal is converted into an electrical signal by the photodiode and subsequently amplified to compensate for

the loop losses. The resulting electrical output can therefore be expressed as:

$$\begin{aligned} V_{\text{out}} = \tfrac{1}{4}P_{\text{in}}.G.S\big\{&\sin^2[mV(t-\tau-T_D)+\phi] \\ &+\sin^2[mV(t-T_D)+\phi] \\ &+2i(t)\sin[mV(t-\tau-T_D)+\phi] \\ &-2q(t)\sin[mV(t-T_D)+\phi]\big\}, \end{aligned} \tag{7}$$

where T_D, G, and S represent the optical fiber delay, amplifier gain, and photodiode sensitivity, respectively, and $i(t) = mI(t)$ and $q(t) = mQ(t)$. The electrical filter in the OEO loop is modeled as a cascade of first-order high-pass and low-pass sections. Its input–output relationship can be written as the integro-differential equation [28] :

$$V_{\text{out}}(t) = V(t) + t_L \frac{dV(t)}{dt} + \frac{1}{t_H}\int_t V(s)\,ds, \tag{8}$$

where $t_L = \frac{1}{\Delta\Omega}$, $t_H = \frac{\Delta\Omega}{\Omega_0^2}$, depend on the filter bandwidth $\Delta\Omega$ and center angular frequency Ω_0. Introducing the normalized variable $x = mV(t)$ and redefining the time as $t' = \frac{t}{t_L}$, together with $y = \frac{1}{t_L}\int x(s)\,ds$, yields the normalized delay-differential model of the system:

$$\begin{aligned} \frac{dx}{dt'} = -\varepsilon y - x + \beta\Big[&\sin^2\big(x(t'-T')+\phi\big) \\ &+ 2i(t')\sin\big(x(t'-T')+\phi\big) + \sin^2\big(x(t'-T)+\phi\big) \\ &- 2q(t')\sin\big(x(t'-T)+\phi\big)\Big], \end{aligned} \tag{9}$$

$$\frac{dy}{dt'} = x. \tag{10}$$

With the introduction of the characteristic time scales t_L and t_H, the model can be expressed in dimensionless form using a reduced set of parameters that govern the dynamical behavior of the OEO. In particular, $\varepsilon = t_L/t_H$ represents the ratio between the low- and high-frequency cutoff time scales, while $T = T_D/t_L$ and $T' = (T_D+\tau)/t_L$ denote the normalized optical and total loop delays, respectively. The normalized feedback gain is defined as $\beta = \pi GSP_{\text{in}}/(2V_\pi)$.

Using these dimensionless parameters, Eqs. (9) and (10) constitute the final normalized model employed throughout the nonlinear dynamical analysis. This formulation incorporates the combined effects of the electro-optic modulation, delayed optical feedback, electrical filtering, and IQ signal injection, and therefore provides the basis for the dynamical analysis.

3 Stability analysis

Equilibrium points are obtained by setting all time derivatives to zero, yielding (x_0, y_0) with $x_0 = 0$ and $y_0 = 2\beta\cos^2\phi/\varepsilon$. We exclude the degenerate case $\phi = \pi/2 \pmod{\pi}$, where the modulator operates at minimum transmission and the linearized dynamics

differ qualitatively. Linearizing around this equilibrium and assuming slowly varying communication signals leads to the characteristic equation :

$$\lambda^2 + \lambda + \varepsilon + \beta \sin(2\phi)\lambda \left(e^{-\lambda T} + e^{-\lambda T'} \right) = 0, \tag{11}$$

where λ denotes the complex eigenvalue associated with the linearized system. The onset of a Hopf bifurcation corresponds to the emergence of a pair of purely imaginary eigenvalues, such that $\lambda = \pm i\omega$, where ω denotes the critical angular frequency. Substituting this condition into the characteristic equation yields the following conditions:

$$\begin{aligned} -\omega^2 + \varepsilon + \beta \sin(2\phi)\, \omega \left[\sin(\omega T) + \sin(\omega T') \right] = 0, \\ 1 + \beta \sin(2\phi) \left[\cos(\omega T) + \cos(\omega T') \right] = 0. \end{aligned} \tag{12}$$

Letting $\gamma = \beta \sin(2\phi)$, the second equation yields $\gamma = -1/[\cos(\omega T) + \cos(\omega T')]$. Substituting into the first and simplifying yields the transcendental equation for the oscillation frequency at threshold:

$$\frac{\varepsilon - \omega_c^2}{\omega_c} = \tan\left[\frac{\omega_c}{2} (T + T') \right]. \tag{13}$$

The corresponding critical feedback gain is

$$\beta_c = -\frac{1}{\sin(2\phi) \left[\cos(\omega_c T) + \cos(\omega_c T') \right]}. \tag{14}$$

The critical feedback gain β_c defines the stability boundary at which the steady-state solution loses stability through a Hopf bifurcation. The critical angular frequency ω_c is determined from Eq. (13), which generally admits multiple branches owing to the periodic dependence of the tangent term. The corresponding feedback threshold is then obtained from Eq. (14), with the physical condition $\beta_c \geq 0$.

To provide a simple interpretation of the critical-frequency condition, two limiting cases are considered [23]. First, assuming $\tan\left(\frac{\omega_c}{2}(T + T')\right) \simeq 0$ gives

$$\omega_c \simeq \sqrt{\varepsilon}. \tag{15}$$

For $\varepsilon = 144$, this approximation gives $\omega_c \simeq 12$. Substitution into Eq. (14) with the selected bias phase $\phi = -3\pi/4$ leads to a negative value of β_c. As a second limiting case, using $\tan\left(\frac{\omega_c}{2}(T + T')\right) \simeq \frac{\omega_c}{2}(T + T')$ in Eq. (13) gives

$$\omega_c \simeq \sqrt{\frac{\varepsilon}{1 + (T + T')/2}}. \tag{16}$$

For the normalized delays considered here, this second approximation also leads to a negative value of β_c. Thus, neither limiting case provides a positive feedback threshold under the selected IQ-modulated operating conditions. In this context, the condition $\beta_c \geq 0$ leads to an effective lower bound $\beta_c = 0$, since the injected IQ waveform already

provides an external excitation of the oscillator and the feedback gain is therefore not required to create an observable forced response.

Notably, if the IQ waveforms were directly injected into the single MZM, they could not also act as external forcing. Therefore, their amplitudes inherently affect the critical frequency and feedback gain, whose expressions can be evaluated through the stability analysis of the amplitude oscillation envelope [29].

4 Results and discussion: nonlinear dynamics under diverse IQ modulation schemes

This section investigates the nonlinear dynamics of the proposed OEO-based joint radar–communication system under different IQ modulation schemes. The objective is to elucidate how the characteristics of the injected communication signals interact with the delayed nonlinear feedback loop to govern the transition between stable and chaotic operating regimes. Particular emphasis is placed on the respective roles of the normalized feedback gain β, the communication bit rates, and the modulation frequencies in shaping the oscillator dynamics. Unless otherwise specified, all simulations are performed with $\varepsilon = 144$, corresponding to a narrowband OEO, a modulator bias phase $\phi = -3\pi/4$, an optical delay $T_D = 20$ ns, and an electrical delay $\tau = 10$ ps.

4.1 Binary IQ modulation

The nonlinear response of the proposed OEO under complementary binary non-return-to-zero (NRZ) IQ modulation is investigated for the communication conditions reported in the experimental architecture of Xue *et al.* [26]. The I and Q channels are modeled as complementary pseudo-random binary sequences operating at bit rates of 181.8 Mb/s and 153.8 Mb/s, respectively, with each symbol remaining constant over one bit period. The resulting dynamical behavior is characterized in Fig. 2 for two representative feedback gains, $\beta = 0.3$ and $\beta = 1$, corresponding to distinct operating regimes of the OEO.

For the lower feedback gain, $\beta = 0.3$, the oscillator remains in a stable periodic regime, as indicated by the single branch of the bifurcation diagram and the negative largest Lyapunov exponent. The corresponding temporal waveform is nearly sinusoidal, while the power spectral density is dominated by a narrow microwave component accompanied by weak harmonic contributions. This behavior reflects the high spectral purity of the generated microwave signal and indicates that the binary IQ excitation does not significantly disturb the regular oscillatory state in this operating condition.

When the feedback gain is increased to $\beta = 1$, a markedly different dynamical behavior is observed. The bifurcation diagram becomes highly spread and the largest Lyapunov exponent takes positive values, indicating the emergence of deterministic chaos. Consistently, the temporal waveform becomes irregular and the power spectral density evolves from a discrete spectrum toward a much broader spectral distribution with a substantially increased background level. The simultaneous modification of the temporal and spectral characteristics confirms that the increase in feedback gain strongly enhances the nonlinear dynamics of the delayed OEO.

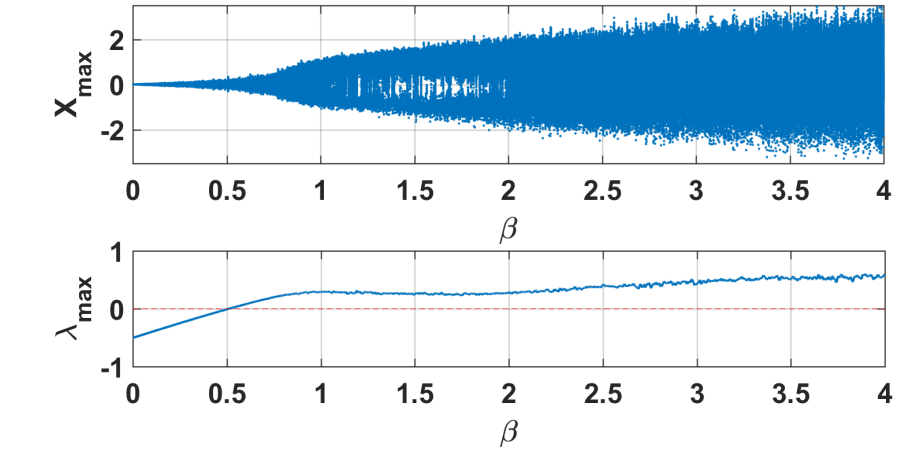
From the JRC perspective, the comparison between $\beta = 0.3$ and $\beta = 1$ illustrates the direct impact of the feedback operating point on the waveform simultaneously used for sensing and communication. At $\beta = 0.3$, the spectrally pure microwave output is favorable for preserving the characteristics of the transmitted I/Q signals and for conventional radar processing. At $\beta = 1$, the broadband chaotic waveform provides increased temporal and spectral complexity, which can be beneficial for waveform diversity in radar applications, while the stronger nonlinear fluctuations may also modify the transmitted I/Q components and affect their recovery at the receiver. Thus, the feedback gain provides an effective means of controlling the balance between spectral purity and nonlinear waveform complexity in the proposed JRC architecture.

To complement the previous bifurcation analysis, the robustness of the proposed architecture is further investigated over the three-dimensional(3D) communication parameter space. Instead of considering a single pair of transmission bit rates, the largest Lyapunov exponent is evaluated for some combinations of the I- and Q-channel bit rates, providing a global assessment of the influence of digital communication on the nonlinear dynamics of the OEO. The resulting dynamic stability maps are presented in Fig. 3.

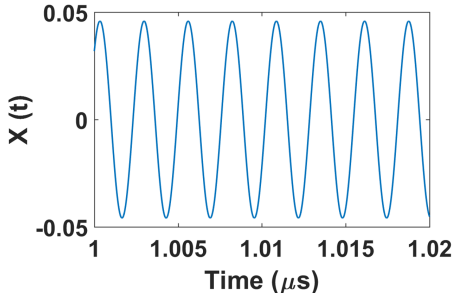
For $\beta = 0.47$, Fig. 3(a), the largest Lyapunov exponent remains negative throughout the investigated bit-rate plane, confirming that variations in the communication rates alone do not destabilize the oscillator. Interestingly, the most negative values of $\lambda_{\max}$ are generally observed toward the higher bit-rate region, indicating that increasing the I- and Q-channel rates does not bring the system closer to instability and may even reinforce the dynamical stability within the investigated range. Thus, stable microwave generation is maintained from low to high transmission rates without requiring a change in the feedback operating point.

A different but equally robust behavior is obtained for $\beta = 3$, Fig. 3(b). The largest Lyapunov exponent remains positive over the entire range of $(50 - 300 Mb/s)$ for both the I- and Q-channel bit rates, confirming that the chaotic regime persists independently of the selected communication rates. However, a progressive reduction of $\lambda_{\max}$ is observed toward higher I- and Q-channel bit rates. The increase in transmission rate therefore modifies the intensity of the chaotic dynamics, but is insufficient to suppress the chaotic regime or restore periodic operation. This result shows that the digital modulation rates influence the strength of the nonlinear response rather than determining its fundamental dynamical state.

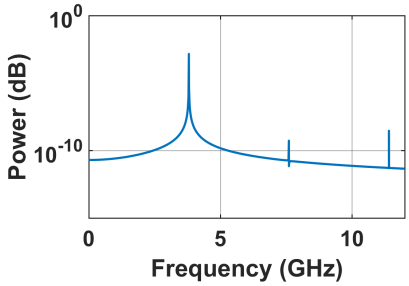
From a joint radar–communication perspective, these results are particularly relevant because they demonstrate that a broad range of communication throughputs can be accommodated without compromising the selected dynamical regime of the OEO. In the stable operating condition, even high bit rates preserve a negative Lyapunov exponent and therefore do not induce unwanted nonlinear instability. In the chaotic operating condition, higher transmission rates slightly reduce the magnitude of the chaotic response while maintaining positive $\lambda_{\max}$, allowing broadband chaotic waveform generation to coexist with high-rate digital modulation. The bit rates can therefore be regarded primarily as communication-performance parameters, while the feedback gain remains the main parameter for selecting the underlying dynamical regime of the JRC system.



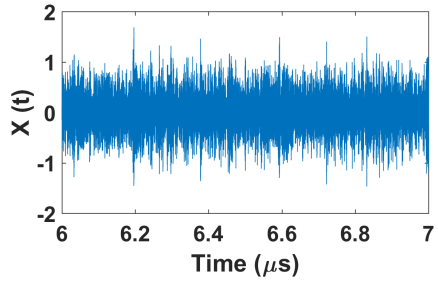
(a)



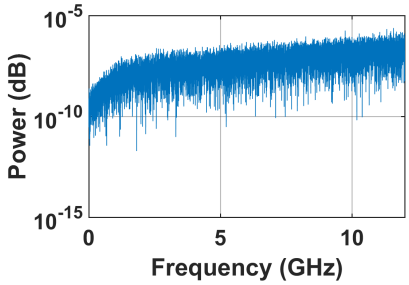
(b)



(c)

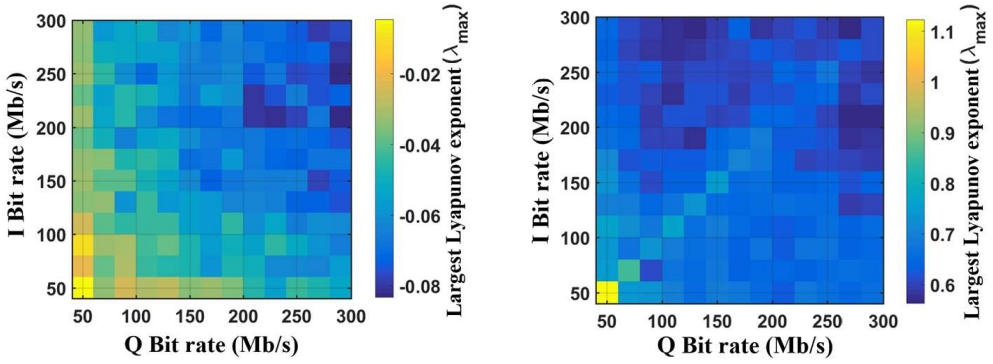


(d)



(e)

Figure 2: (a) Bifurcation diagram and maximum Lyapunov exponent as a function of the normalized feedback gain β under complementary binary NRZ IQ modulation, with I- and Q-channel bit rates of 181.8 Mb/s and 153.8 Mb/s, respectively; (b)–(c) Temporal trace and power spectral density for $\beta = 0.3$; (d)–(e) Temporal trace and power spectral density for $\beta = 1$.



(a) (b)

Figure 3: Dynamic stability maps of the system under binary IQ modulation. The color scale represents the largest Lyapunov exponent ($\lambda_{\max}$). (a) Binary IQ modulation with $\beta = 0.47$; (b) Binary IQ modulation with $\beta = 3$.

4.2 Sinusoidal IQ modulation with identical frequencies ($f_I = f_Q = 5$ GHz)

The analysis is now extended to continuous sinusoidal IQ excitation in order to examine how a deterministic communication waveform modifies the nonlinear dynamics of the proposed OEO. In this configuration, the in-phase and quadrature signals are described by two orthogonal sinusoidal waveforms,

$$I(t) = 3\sin(2\pi f_I t), \tag{17}$$

$$Q(t) = 3\cos(2\pi f_Q t), \tag{18}$$

where $f_I = f_Q = 5$ GHz. This configuration corresponds to the conventional IQ scheme in which both channels share the same carrier frequency while remaining in phase quadrature.

The corresponding nonlinear dynamics are presented in Fig. 4. Compared with the binary IQ case, the evolution toward chaos is considerably more gradual. As shown in Fig. 4(a), the largest Lyapunov exponent increases progressively with the feedback gain and becomes positive at approximately $\beta \approx 1.2$, indicating the onset of deterministic chaotic dynamics at a substantially higher feedback level than that observed for binary excitation.

The temporal and spectral responses provide further evidence of this progressive transition. For $\beta = 0.6$, the OEO remains in a regular oscillatory regime, with a nearly sinusoidal temporal waveform and a power spectral density dominated by a narrow component at 5 GHz together with a weaker second harmonic at 10 GHz. As the feedback gain is increased to $\beta = 2$, the temporal waveform becomes irregular and a broadband spectral background emerges, consistently with the positive Lyapunov exponent. Nevertheless, the spectral components around 5 GHz and 10 GHz remain

clearly identifiable. Thus, the onset of chaotic dynamics does not immediately suppress the frequency components imposed by the sinusoidal excitation; instead, the original spectral structure is progressively embedded within a broader nonlinear background.

This behavior distinguishes the sinusoidal excitation from the binary case and is particularly relevant to the subsequent frequency-dependent analysis. The coexistence of identifiable carrier components with broadband nonlinear spectral content indicates that the OEO can retain information about the imposed IQ excitation while entering a chaotic regime. The degree to which this spectral coexistence can be exploited for signal separation depends on the selected operating point and motivates the investigation of unequal I- and Q-channel frequencies in the following subsection.

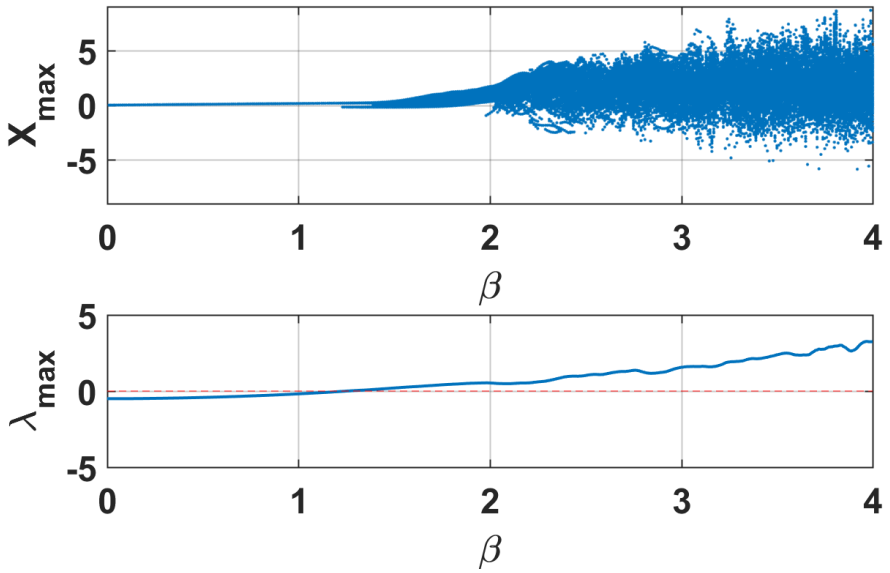
4.3 Sinusoidal IQ modulation with different frequencies ($f_Q = 3$ GHz, $f_I = 5$ GHz)

The analysis is further extended to a frequency-diverse sinusoidal IQ configuration in which the I- and Q-channel signals are assigned different carrier frequencies. Accordingly, the sinusoidal waveforms defined by Eqs. (17) and (18) are considered with $f_I = 5$ GHz and $f_Q = 3$ GHz. This configuration introduces a frequency separation between the two channels and provides an additional degree of freedom for investigating the interaction between the injected waveforms and the delayed nonlinear dynamics of the OEO.

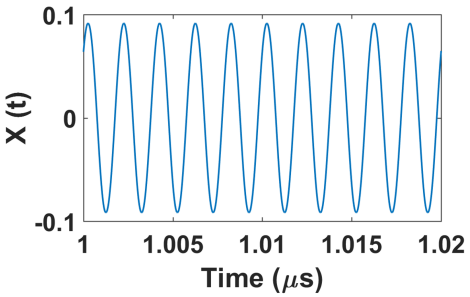
The corresponding bifurcation diagram and largest Lyapunov exponent are presented in Fig. 5(a). The oscillator remains in a stable periodic regime over a substantially extended range of feedback gain, with the largest Lyapunov exponent remaining close to zero or negative up to approximately $\beta \approx 3$. Beyond this region, $\lambda_{\max}$ increases rapidly and becomes positive, indicating the development of chaotic dynamics. Compared with the identical-frequency configuration, the onset of chaos is therefore shifted toward higher feedback gains, showing that the frequency allocation of the IQ excitation has a measurable influence on the nonlinear stability of the OEO.

The temporal and spectral responses provide further insight into this behavior. At $\beta = 1.5$, the temporal waveform in Fig. 5(b) exhibits a regular beating pattern resulting from the superposition of the two sinusoidal components. The corresponding power spectral density in Fig. 5(c) presents distinct spectral components associated with the injected frequencies, together with additional peaks generated by the nonlinear response of the feedback loop. In particular, the presence of multiple components distributed over the microwave spectrum indicates that the interaction between the 3- and 5-GHz excitations produces harmonic and intermodulation products, rather than simply reproducing the two injected frequencies. This spectral enrichment becomes considerably more pronounced when the feedback gain is increased to $\beta = 4$. As shown in Fig. 5(d)–(e), the temporal waveform becomes strongly irregular and the spectrum evolves into a broad continuous background populated by numerous spectral components, which is consistent with the positive Lyapunov exponent observed in Fig. 5(a).

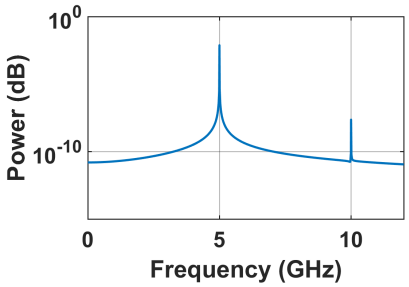
Despite this spectral broadening, the frequency components associated with the injected IQ excitation remain embedded within the generated microwave spectrum. The results therefore show that frequency-diverse excitation affects not only the stability



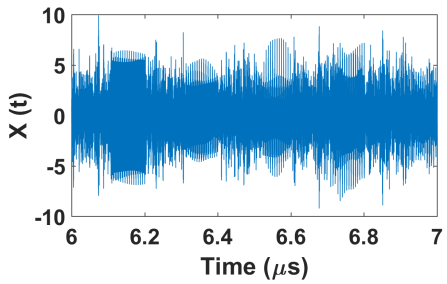
(a)



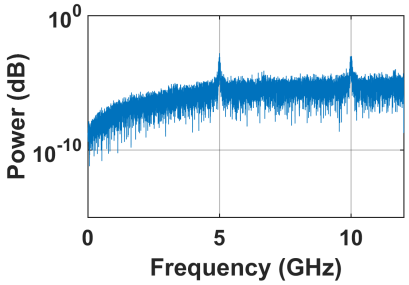
(b)



(c)



(d)



(e)

Figure 4: (a) Bifurcation diagram and maximum Lyapunov exponent as a function of β for sinusoidal IQ modulation with $f_I = f_Q = 5$ GHz; (b)–(c) temporal trace and power spectral density for $\beta = 0.6$; (d)–(e) temporal trace and power spectral density for $\beta = 2$.

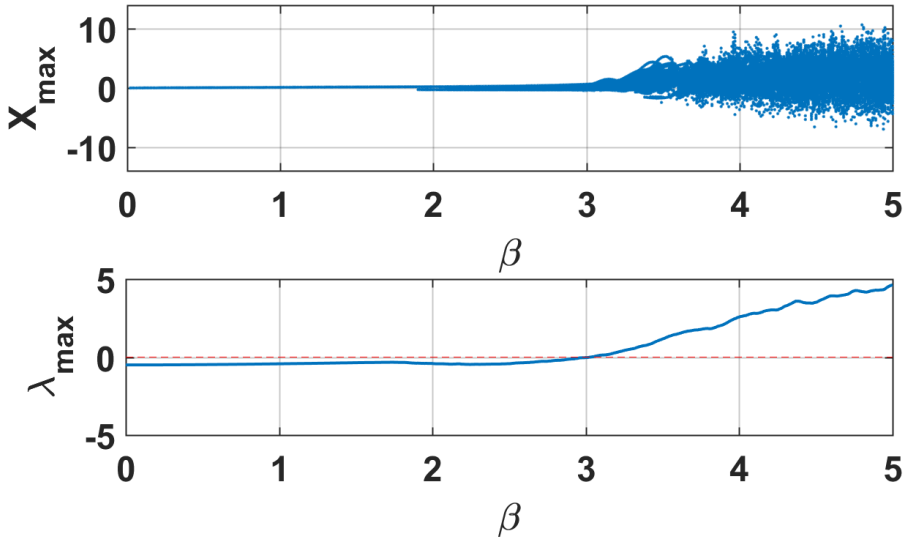
boundary of the OEO but also the spectral organization of the generated waveform. From a JRC perspective, this behavior is of particular interest because the frequency separation between the I- and Q-channel excitations can be exploited to distinguish the information-bearing components, while the nonlinear feedback simultaneously generates additional spectral content that can contribute to waveform diversity. The choice of (f_I, f_Q) thus provides a means of balancing dynamical stability, spectral diversity, and channel separability within the same photonic platform.

To complement the previous one-dimensional bifurcation analysis, the influence of the sinusoidal IQ excitation is investigated over the three-dimensional modulation-frequency space. The largest Lyapunov exponent is evaluated for combinations of the I- and Q-channel frequencies while keeping the feedback gain fixed. The resulting dynamic stability maps, presented in Fig. 6, provide a global representation of the operating regimes and reveal that the modulation frequencies can directly influence the nonlinear state of the OEO.

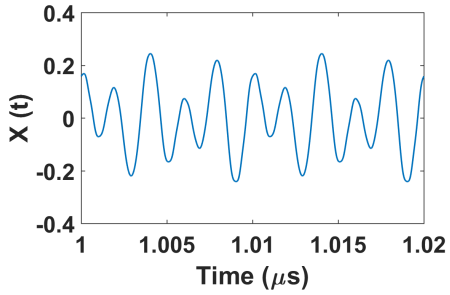
For the moderate feedback gain ($\beta = 0.5$), Fig. 6(a) reveals a coexistence of stable and chaotic regions within the investigated (f_I, f_Q) plane. Negative values of $\lambda_{\max}$ are mainly concentrated in the low-frequency region, with the most pronounced stable domains occurring for specific combinations of f_I and f_Q. As the modulation frequencies are increased, $\lambda_{\max}$ progressively approaches and exceeds zero over a larger portion of the parameter space, indicating a transition toward chaotic operation. Importantly, the stability is not governed by either frequency independently, but by their combined influence on the delayed nonlinear dynamics. Thus, unlike binary IQ modulation, the carrier frequencies of sinusoidal IQ excitation act as effective control parameters that can reshape the dynamical operating regime of the OEO.

A markedly different behavior is observed for the larger feedback gain ($\beta = 4$), shown in Fig. 6(b). The entire investigated frequency plane exhibits positive largest Lyapunov exponents, confirming that the oscillator remains in a developed chaotic regime over the considered range of f_I and f_Q. The gradual variation of $\lambda_{\max}$ across the frequency plane indicates that the modulation frequencies still influence the intensity of the chaotic dynamics, even though they no longer restore a stable operating region. In this regime, the feedback-induced nonlinear dynamics therefore remain dominant over the variations introduced by the sinusoidal excitation frequencies.

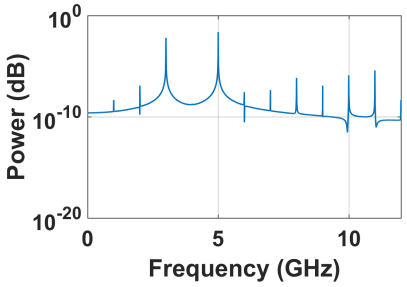
From a JRC perspective, these maps provide a useful system-level view of how the communication waveform can be incorporated into the dynamical design of the OEO. At moderate feedback gain, the existence of stable regions offers operating points where the sinusoidal I/Q signals can be generated while maintaining a regular microwave response, whereas regions with positive $\lambda_{\max}$ provide access to broadband chaotic operation. At higher feedback gain, the persistence of positive Lyapunov exponents over the complete frequency range indicates that chaotic operation is robust against changes in the selected carrier frequencies. Consequently, the (f_I, f_Q) maps provide a practical means of identifying frequency combinations compatible with the desired dynamical regime and of assessing the robustness of the OEO-based JRC operation with respect to the selected communication frequencies.



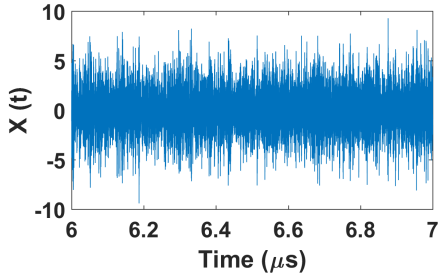
(a)



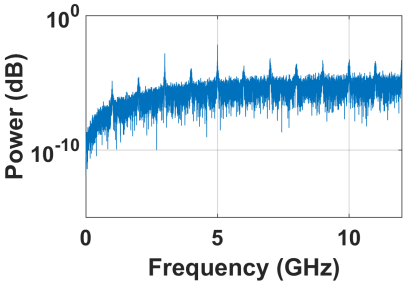
(b)



(c)

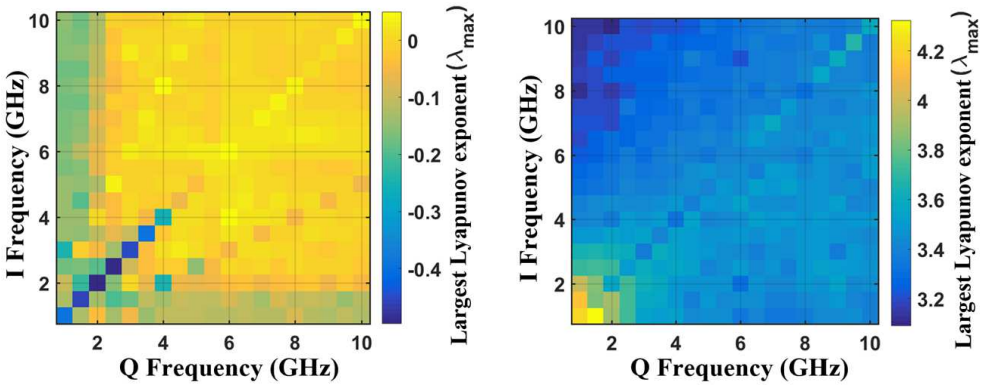


(d)



(e)

Figure 5: (a) Bifurcation diagram and maximum Lyapunov exponent as a function of β for $f_I = 5$ GHz and $f_Q = 3$ GHz; (b)–(c) Temporal trace and power spectral density for $\beta = 1.5$; (d)–(e) Temporal trace and power spectral density for $\beta = 4$.



(a) (b)

Figure 6: Dynamic stability maps of the system under sinusoidal IQ modulation. The color scale represents the largest Lyapunov exponent ($\lambda_{\max}$). (a) Sinusoidal IQ modulation with $\beta = 0.5$; and (b) Sinusoidal IQ modulation with $\beta = 4$.

4.4 Design implications for OEO-based joint radar–communication systems

The results obtained for the different IQ modulation schemes provide a clear picture of how the communication waveform and the feedback gain jointly determine the operating regime of the OEO-based JRC system. While the feedback gain primarily controls the transition between stable and chaotic operation, the influence of the communication parameters depends strongly on the modulation format.

For binary IQ modulation, varying the I- and Q-channel bit rates over the investigated range produces only minor changes in the largest Lyapunov exponent and does not alter the overall dynamical regime imposed by the feedback gain. This indicates that the communication rate can be adjusted over a broad range without requiring a corresponding modification of the OEO operating point. From a JRC perspective, this provides flexibility in adapting the communication throughput while maintaining the selected microwave-generation regime.

Sinusoidal IQ modulation exhibits a different behavior, since the carrier frequencies directly affect the stability landscape of the oscillator. The three-dimensional frequency maps show that stable and chaotic operating regions can coexist for moderate feedback gain, allowing the dynamical regime to be influenced through the choice of (f_I, f_Q). When the two channels are assigned different frequencies, the resulting spectral components remain identifiable even as the oscillator enters the chaotic regime, providing an additional degree of freedom for separating the communication components from the broadband microwave waveform.

These results suggest that the selection of the operating point should be based on the desired balance between dynamical stability, spectral characteristics, and

communication requirements. Stable operation is advantageous when spectral purity and faithful signal recovery are prioritized, whereas chaotic operation provides a broadband and dynamically rich waveform that can be exploited for radar-oriented functionalities. Within this framework, the feedback gain determines the principal dynamical regime, while the IQ modulation parameters provide additional means of adapting the generated waveform to the requirements of the JRC system.

5 Conclusion

This paper has presented a comprehensive analytical and numerical investigation of the nonlinear dynamics of an optoelectronic oscillator (OEO)-based joint radar–communication (JRC) architecture under binary and sinusoidal IQ modulation. A delay-differential model was established and combined with linear stability analysis to derive the critical oscillation frequency and feedback gain. These analytical results provided a reference for the subsequent nonlinear investigation, which was performed using bifurcation diagrams, the largest Lyapunov exponent, time-domain responses, power spectral density, and three-dimensional dynamic stability maps.

The results demonstrate that the nonlinear behavior of the OEO is governed by the combined effects of the feedback gain and the characteristics of the injected communication waveforms. While the feedback gain remains the dominant parameter controlling the transition between stable and chaotic operation, binary IQ modulation exhibits a limited sensitivity to the communication bit rates over the investigated range. In contrast, sinusoidal IQ modulation introduces the I- and Q-channel frequencies as additional parameters that reshape the dynamical stability landscape. In particular, using distinct carrier frequencies enlarges the stable operating region and preserves identifiable spectral components, providing favorable conditions for the spectral separation and processing of the transmitted signals.

Overall, the results show that the communication waveform is an active component of the nonlinear dynamics of the OEO rather than merely an information-bearing input. The combined analytical stability analysis and three-dimensional dynamical maps therefore provide a systematic framework for relating communication parameters to the nonlinear operating regime of the OEO. This establishes clear design guidelines for selecting the feedback gain and IQ modulation parameters according to the required balance between spectral purity, dynamical stability, and broadband waveform generation in OEO-based JRC systems.

Funding

The authors would like to thank Conselho Nacional de Desenvolvimento Científico e Tecnológico (CNPq) under the grant 403784/2023-9 for the partial funding of this research.

References

[1] Bishop, R.: Intelligent vehicle technology and trends. IEEE Instrumentation & Measurement Magazine **9**(1), 54–54 (2006)

[2] Paul, B., Chiriyath, A.R., Bliss, D.W.: Survey of rf communications and sensing convergence research. IEEE Access **5**, 252–270 (2016)

[3] Kumari, P., Choi, J., González-Prelcic, N., Heath, R.W.: Ieee 802.11 ad-based radar: An approach to joint vehicular communication-radar system. IEEE Transactions on Vehicular Technology **67**(4), 3012–3027 (2017)

[4] Gyawali, S., Xu, S., Qian, Y., Hu, R.Q.: Challenges and solutions for cellular based v2x communications. IEEE Communications Surveys & Tutorials **23**(1), 222–255 (2020)

[5] Hassanien, A., Amin, M.G., Zhang, Y.D., Ahmad, F.: Signaling strategies for dual-function radar communications: An overview. IEEE Aerospace and Electronic Systems Magazine **31**(10), 36–45 (2016)

[6] Zhang, L., Zhao, H., Hou, S., Zhao, Z., Xu, H., Wu, X., Wu, Q., Zhang, R.: A survey on 5g millimeter wave communications for uav-assisted wireless networks. IEEE Access **7**, 117460–117504 (2019)

[7] Dokhanchi, S.H., Mysore, B.S., Mishra, K.V., Ottersten, B.: A mmwave automotive joint radar-communications system. IEEE Transactions on Aerospace and Electronic Systems **55**(3), 1241–1260 (2019)

[8] Li, Q., Dai, K., Zhang, Y., Zhang, H.: Integrated waveform for a joint radar-communication system with high-speed transmission. IEEE Wireless Communications Letters **8**(4), 1208–1211 (2019)

[9] Hassanien, A., Amin, M.G., Aboutanios, E., Himed, B.: Dual-function radar communication systems: A solution to the spectrum congestion problem. IEEE Signal Processing Magazine **36**(5), 115–126 (2019)

[10] Cao, N., Chen, Y., Gu, X., Feng, W.: Joint bi-static radar and communications designs for intelligent transportation. IEEE Transactions on Vehicular Technology **69**(11), 13060–13071 (2020)

[11] Yao, X.S., Maleki, L.: Optoelectronic microwave oscillator. Journal of the Optical Society of America B **13**(8), 1725–1735 (1996)

[12] Ferreira, V.T., Magri, V.P., Santos, A.C., Ribeiro, R.M.: Optoelectronic oscillator using visible leds and plastic optical fibers. Applied Optics **63**(34), 8796–8801 (2024)

[13] Talla Mbé, J.H., Kamaha, J.S., Chembo, Y.K., Woafo, P.: Dynamics of wideband time-delayed optoelectronic oscillators with nonlinear filters. IEEE Journal of Quantum Electronics **55**(4), 1–6 (2019)

[14] Chembo, Y.K.: Laser-based optoelectronic generation of narrowband microwave

chaos for radars and radio-communication scrambling. Optics Letters **42**(17), 3431–3434 (2017)

[15] Yang, B., Sun, J., Chi, H., Xu, K., Yang, S.: Joint radar and communication system based on a chaotic optoelectronic oscillator. Optics Communications **554**, 130123 (2024)

[16] Xiong, H., Jiang, N., Li, A., Che, M., Wang, C., Zhang, Q., Zhang, Y., Qiu, K.: Chaotic optoelectronic oscillators-based dual-function radar-communication system. Science China Information Sciences **68**(9), 192302 (2025)

[17] Yao, J.: Optoelectronic oscillators for high speed and high resolution optical sensing. Journal of lightwave technology **35**(16), 3489–3497 (2017)

[18] Pefireko, A.B.N., Talla Mbé, J.H.: Theoretical investigation of physical parameters measurements of a liquid in a vessel using optoelectronic oscillators. Optical and Quantum Electronics **55**(9), 782 (2023)

[19] Koualong, M.T., Talla Mbé, J.H., Tatietse, T.T.: Efficient sensings of temperature, refractive index, and distance measurement using the cubic-nonlinear optoelectronic oscillators. Optical and Quantum Electronics **54**(5), 311 (2022)

[20] Atchoffo, W.N., Talla Mbé, J.H., Woafo, P., Tchitnga, R.: Time-delay signature suppression in single loop optoelectronic oscillators based on sine hyperbolic nonlinear amplifier. Optical & Quantum Electronics **55**(4), 1 (2023)

[21] Chembo, Y., Larger, L., Tavernier, H., Bendoula, R., Rubiola, E., Colet, P.: Dynamic instabilities of microwaves generated with optoelectronic oscillators. Optics letters **32**(17), 2571–2573 (2007)

[22] Talla Mbé, J.H., Talla, A.F., Chengui, G.R.G., Coillet, A., Larger, L., Woafo, P., Chembo, K.Y.: Mixed-mode oscillations in slow-fast delayed optoelectronic systems. Physical review E **91**(1), 012902–6 (2015)

[23] Talla Mbé, J.H., Chiajeu Njidjou, M., Talla, A.F., Woafo, P., Chembo, Y.K.: Multistability, relaxation oscillations, and chaos in time-delayed optoelectronic oscillators with direct laser modulation. Optics Letters **49**(5), 1277–1280 (2024)

[24] Sinquin, B., Romanelli, M., Bouhier, S., Frein, L., Alouini, M., Vallet, M.: Low phase noise direct-modulation optoelectronic oscillator. Journal of Lightwave Technology **39**(24), 7788–7793 (2021)

[25] Zeng, Z., Zhang, L., Wu, Y., Zhang, Z., Zhang, S., Zhang, Y., Sun, B., Liu, Y.: Multi-format microwave signal generation based on an optoelectronic oscillator. Optics express **29**(19), 30834–30843 (2021)

[26] Xue, Z., Li, S., Xue, X., Zheng, X., Zhou, B.: Photonics-assisted joint radar

and communication system based on an optoelectronic oscillator. Optics Express **29**(14), 22442–22454 (2021)

[27] Zhang, F., Ge, X., Pan, S.: Triangular pulse generation using a dual-parallel mach–zehnder modulator driven by a single-frequency radio frequency signal. Optics Letters **38**(21), 4491–4493 (2013)

[28] Chembo, Y.K., Larger, L., Colet, P.: Nonlinear dynamics and spectral stability of optoelectronic microwave oscillators. IEEE journal of quantum electronics **44**(9), 858–866 (2008)

[29] Dai, H., Chembo, Y.K.: Classification of iq-modulated signals based on reservoir computing with narrowband optoelectronic oscillators. IEEE Journal of Quantum Electronics **57**(3), 1–8 (2021)